

Article

Identification of Bacterial Metabolites Modulating Breast Cancer Cell Proliferation and Epithelial-Mesenchymal Transition

Gyula Ujlaki ¹, Tünde Kovács ¹, András Vida ¹, Endre Kókai ¹, Boglára Rauch ¹, Szandra Schwarcz ¹, Edit Mikó ¹, Eszter Janka ², Adrienn Sipos ¹, Csaba Hegedűs ¹, Karen Uray ¹, Péter Nagy ³
and Peter Bai ^{1,4,5,6,*}

- ¹ Department of Medical Chemistry, Faculty of Medicine, University of Debrecen, 4032 Debrecen, Hungary; ujlaki.gyula@med.unideb.hu (G.U.); kovacs60.tunde90@gmail.com (T.K.); avida@foss.dk (A.V.); ekokai@med.unideb.hu (E.K.); rauch.boglarka@med.unideb.hu (B.R.); schwarcz.szandra@med.unideb.hu (S.S.); miko.edit@med.unideb.hu (E.M.); siposadri@med.unideb.hu (A.S.); hcsaba@med.unideb.hu (C.H.); karen.uray@med.unideb.hu (K.U.)
- ² Department of Dermatology, Faculty of Medicine, University of Debrecen, 4032 Debrecen, Hungary; janka.eszter.a@gmail.com
- ³ Department of Biophysics and Cell Biology, Faculty of Medicine, University of Debrecen, 4032 Debrecen, Hungary; nagyp@med.unideb.hu
- ⁴ MTA-DE Lendület Laboratory of Cellular Metabolism, 4032 Debrecen, Hungary
- ⁵ Research Center for Molecular Medicine, Faculty of Medicine, University of Debrecen, 4032 Debrecen, Hungary
- ⁶ ELKH-DE Cell Biology and Signaling Research Group ELKH, 4032 Debrecen, Hungary
- * Correspondence: baip@med.unideb.hu; Tel.: +36-52-412345; Fax: +36-52-412566

Abstract: Breast cancer patients are characterized by the oncobiogenic transformation of multiple microbiome communities, including the gut microbiome. Oncobiogenic transformation of the gut microbiome impairs the production of antineoplastic bacterial metabolites. The goal of this study was to identify bacterial metabolites with antineoplastic properties. We constructed a 30-member bacterial metabolite library and screened the library compounds for effects on cell proliferation and epithelial-mesenchymal transition. The metabolites were applied to 4T1 murine breast cancer cells in concentrations corresponding to the reference serum concentrations. However, yric acid, glycolic acid, D-mannitol, 2,3-butanediol, and trans-ferulic acid exerted cytostatic effects, and 3-hydroxyphenylacetic acid, 4-hydroxybenzoic acid, and vanillic acid exerted hyperproliferative effects. Furthermore, 3-hydroxyphenylacetic acid, 4-hydroxybenzoic acid, 2,3-butanediol, and hydrocinnamic acid inhibited epithelial-to-mesenchymal (EMT) transition. We identified redox sets among the metabolites (D-mannitol—D-mannose, 1-butanol—butyric acid, ethylene glycol—glycolic acid—oxalic acid), wherein only one partner within the set (D-mannitol, butyric acid, glycolic acid) possessed bioactivity in our system, suggesting that changes to the local redox potential may affect the bacterial secretome. Of the nine bioactive metabolites, 2,3-butanediol was the only compound with both cytostatic and anti-EMT properties.

Keywords: high content screening; butyric acid; vanillic acid; glycolic acid; D-mannitol; trans-ferulic acid; 2,3-butanediol; 4-hydroxybenzoic acid; hydrocinnamic acid; 3-hydroxyphenylacetic acid; epithelial-mesenchymal transition; proliferation; bacterial metabolite; dysbiosis; breast cancer; metabolite signaling; microbiome; secretome



Citation: Ujlaki, G.; Kovács, T.; Vida, A.; Kókai, E.; Rauch, B.; Schwarcz, S.; Mikó, E.; Janka, E.; Sipos, A.; Hegedűs, C.; et al. Identification of Bacterial Metabolites Modulating Breast Cancer Cell Proliferation and Epithelial-Mesenchymal Transition. *Molecules* **2023**, *28*, 5898. <https://doi.org/10.3390/molecules28155898>

Academic Editor: Jean-Marc Sabatier

Received: 30 June 2023

Revised: 27 July 2023

Accepted: 2 August 2023

Published: 5 August 2023



Copyright: © 2023 by the authors. Licensee MDPI, Basel, Switzerland. This article is an open access article distributed under the terms and conditions of the Creative Commons Attribution (CC BY) license (<https://creativecommons.org/licenses/by/4.0/>).

1. Introduction

Breast cancer is the most frequent cancer in women [1,2]. Breast cancer is characterized by the disturbance of multiple microbiome compartments, termed oncobiosis [3]. Oncobiosis affects the microbiomes of breast tissue [4,5], milk ducts [6], the tumor's inherent microbiome [7–21], the distal gut [22–42], and the urinary tract [13,43]. Oncobiosis support of breast tumors is multifaceted. (1) Bacteria colonize the tumor tissue; (2) the immune

system favors the tolerogenic state [44]; and (3) the gut microbiome's capacity to produce antitumor metabolites is suppressed [29–31,45–47].

The gut microbiome has a large capacity to produce a diverse set of bioactive metabolites. These low-molecule-weight biomolecules can enter the systemic circulation and reach different cell types in the human body, including cancer cells. This process is similar to the action of hormones or paracrine signaling molecules. The first such “metabolite” was identified more than 50 years ago [48] using the observation that the gut oncobiome in breast cancer has a larger capacity to reactivate conjugated estrogens via beta-glucuronidases than the gut eubiome. Multiple cytostatic metabolites produced by the gut eubiome have been identified in breast cancer, including lithocholic acid [29,49], cadaverine [30], indole metabolites [31,32], and short-chain fatty acids [50,51]. These metabolites exert antineoplastic effects, including modulation of cell proliferation and epithelial-mesenchymal transition (EMT) [44]. As stated earlier, the metabolic capacity of the microbiome is suppressed in breast cancer, and the capacity to produce known antineoplastic metabolites decreases in breast cancer [29–31,45–47].

Given the enormous and diverse metabolic capacity of the (gut) microbiome, other bacterial metabolites may also possess biological activity toward breast cancer cells. The goal of this study was to identify bacterial metabolites with antineoplastic activities in breast cancer.

2. Results

2.1. Metabolite Library Construction

Bacterial metabolites that interfere with human metabolism were identified via a literature search. The metabolites identified using this search were curated to eliminate falsely identified metabolites (i.e., not produced in bacteria). The serum reference concentration of the metabolites was established using literature searches (see Table 1).

A recent report [82] showed that tumors impact gut motility by modulating beta-adrenergic receptors. Varying the speed of passage likely changes the redox environment of the GI tract [83], suggesting that the redox state of redox-labile metabolites may change in breast cancer patients. Therefore, the redox partner of the applicable metabolites (mannose—D-mannitol, TMA—TMAO, 1-butanol—butyric acid, ethylene glycol—glycolic acid, oxalic acid) was introduced into the library, and the serum reference concentrations were established using a literature search. The literature search did not yield results for ethylene glycol; therefore, the same concentration was used as the redox partner with a known reference concentration. The metabolites, serum reference concentrations, treatment concentrations, and corresponding literature are listed in Table 1.

2.2. Development of High-Throughput Methods for Assessing Cell Proliferation

In previous studies, we identified and characterized a set of bacterial metabolites with cytostatic activity [29–32]; however, the antiproliferative activity of the metabolites was limited, and the SRB proliferation assay was not ideal for obtaining high-precision data under these conditions. Therefore, we tested two Image-analysis-based nuclei counting methods. Image segmentation and nuclei counting were performed using CellProfiler in one method, and segmentation was performed using a deep learning (DL)-based method developed by us, followed by nuclei counting using CellProfiler in the second method.

The SRB assay was unreliable at low cell densities in the range of 100–300 cells/well. Furthermore, due to the inherent limitations of photometry, values above an absorbance of 1.0 are not reliable, limiting the maximum number of cells that can be measured to 10,000–30,000 cells (Figure 1A). Values above an absorbance of 1.0 can be measured after dilution, which may introduce errors. Image-analysis-based assays have a larger dynamic range than the SRB assay. Both image-analysis-based assays were reliable for measuring low cell numbers (Figure 1A). The analysis-based assays were also able to detect up to 100,000 cells/well. On the high end of the scale, the DL-based method was superior to the CellProfiler's built-in method (Figure 1A). In contrast to conventional methods, semantic

segmentation models do not require parameter adjustment for every run. Of note, the image-analysis-based assays identified fewer cells than introduced if the number of plated cells was 1000–10,000. Visual inspection of the wells revealed that, at these densities, cells adhered less to plates, leading to lower cell numbers. Hence, cell numbers did indeed decrease in the culture plates (Figure 1B), suggesting that the image-analysis-based assays are precise. Based on these results, we applied the image-analysis-based assays in subsequent experiments.

Table 1. The specifics of the metabolites introduced to the metabolite library.

	Metabolite Name	Solvent	Catalog Number	Serum Reference Concentrations (μM)	Applied Concentrations (μM)
1	1-Butanol	PBS	Sigma B7906-500ML	0–0.27 [52]	0.005, 0.015, 0.044, 0.13, 0.4
2	1-Propanol	PBS	Sigma 96566-5ML-F	0–0.8 [52]	0.05, 0.1, 0.2, 0.4, 0.8
3	2,3-butanediol	PBS	Sigma B84904	0.5–0.9 [53]	0.48, 0.56, 0.66, 0.77, 0.9
4	3,4-dihydroxyphenyl acetic acid	PBS	Sigma 850217-14	0.0102–0.104 [54,55]	0.01, 0.018, 0.032, 0.058, 0.104
5	3-Hydroxyphenylacetic acid	PBS	Sigma H49901	0.11–0.174 [54]	0.106, 0.120, 0.136, 0.154, 0.174
6	3-Hydroxypropionic acid	PBS	Sigma 792659-1G	3, 6, 8 (individual values) [56]	0.5, 1, 2, 4, 8
7	4-aminobenzoic acid	EtOH	Sigma A9878-5G	5.01–32.0 [57]	0.3, 1.2, 3.6, 10.8, 32.4
8	4-hydroxybenzoic acid	PBS	Sigma 8218140250	0.019–0.035 [54]	0.019, 0.022, 0.026, 0.03, 0.035
9	4-Hydroxyphenylacetic acid	PBS	Sigma H50004-54	0.283–0.61 [54]	0.28, 0.36, 0.41, 0.5, 0.61
10	Acetic acid	PBS	VWR UN2789	23–254.4 [52,58–61]	15, 30, 60, 120, 240
11	Allantoin	DMSO	Sigma 05670	1.0–24.0 [62–64]	0.99, 2.2, 4.9, 10.8, 24
12	Butyric acid	PBS	Sigma B103500-5ML	1.39–14.15 [59–61]	1, 2, 4, 8, 16
13	D-alanine	PBS	Sigma A7377-5G	0–0.77 [65]	0.048, 0.96, 0.193, 0.385, 0.77
14	D-glutamic acid	PBS	Sigma G1001-1G	7.42–14.6 [65]	7.28, 8.66, 10.31, 12.27, 14.6
15	D-mannitol	PBS	Sigma M4125-10MG	no report, same concentrations as for D-mannose	6.25, 12.5, 25, 50, 100
16	D-mannose	DMSO	no data	13–73.87 [66–68]	6.25, 12.5, 25, 50, 100
17	Ethylene glycol	PBS	no data	no data, toxic (1.56 mg/kg)	1, 3, 9, 27, 81
18	Formic acid	PBS	Sigma F0507-500ML	11.84–224.5 [69]	10, 30, 90, 270, 810
19	Glycolic acid	PBS	Sigma 124737	6.1–69 [56,70]	1, 3, 9, 27, 81
20	Hippuric acid	PBS	Sigma 112003	1.5–21.2 [54,71]	0.024, 0.12, 0.6, 3, 15
21	Hydrocinnamic acid	EtOH	Sigma 135232-5G	0.131–0.354 [72]	0.128, 0.165, 0.213, 0.274, 0.354
22	Isobutyric acid	PBS	Sigma I1754-100ML	1.02–14.15 [59,61]	1.02, 1.97, 3.80, 7.33, 14.15
23	L-pipecolic acid	PBS	Sigma P2519	1.2–3.72 [73]	0.25, 0.5, 1, 2, 4
24	oxalic acid	PBS	Sigma 75688	6.5–35.5 [74,75]	6.5, 9.9, 15.2, 23.2, 35.5
25	Propionic acid	PBS	Sigma P1386-1L	4.86–15.33 [59–61]	1.25, 2.5, 5, 10, 20
26	Shikimic acid	DMSO	Sigma S5375-10MG	0.03–0.23 [76]	0.01, 0.03, 0.09, 0.27, 0.81
27	trans-ferulic acid	DMSO	Sigma 52229	0.04–15.7 [54,71]	0.016, 0.08, 0.4, 2, 10
28	Trimethylamine (TMA)	PBS	Sigma 92260	0.3–14.44 [77,78]	0.3, 0.79, 2.1, 5.4, 14.35
29	Trimethylamine-N-oxide (TMAO)	PBS	Sigma 317594	1.21–21.1 [79–81]	1.22, 2.48, 5.065, 10.33, 21.1
30	Vanillic acid	PBS	Sigma H36001	0.01–0.338 [54,71]	0.01, 0.024, 0.058, 0.140, 0.338

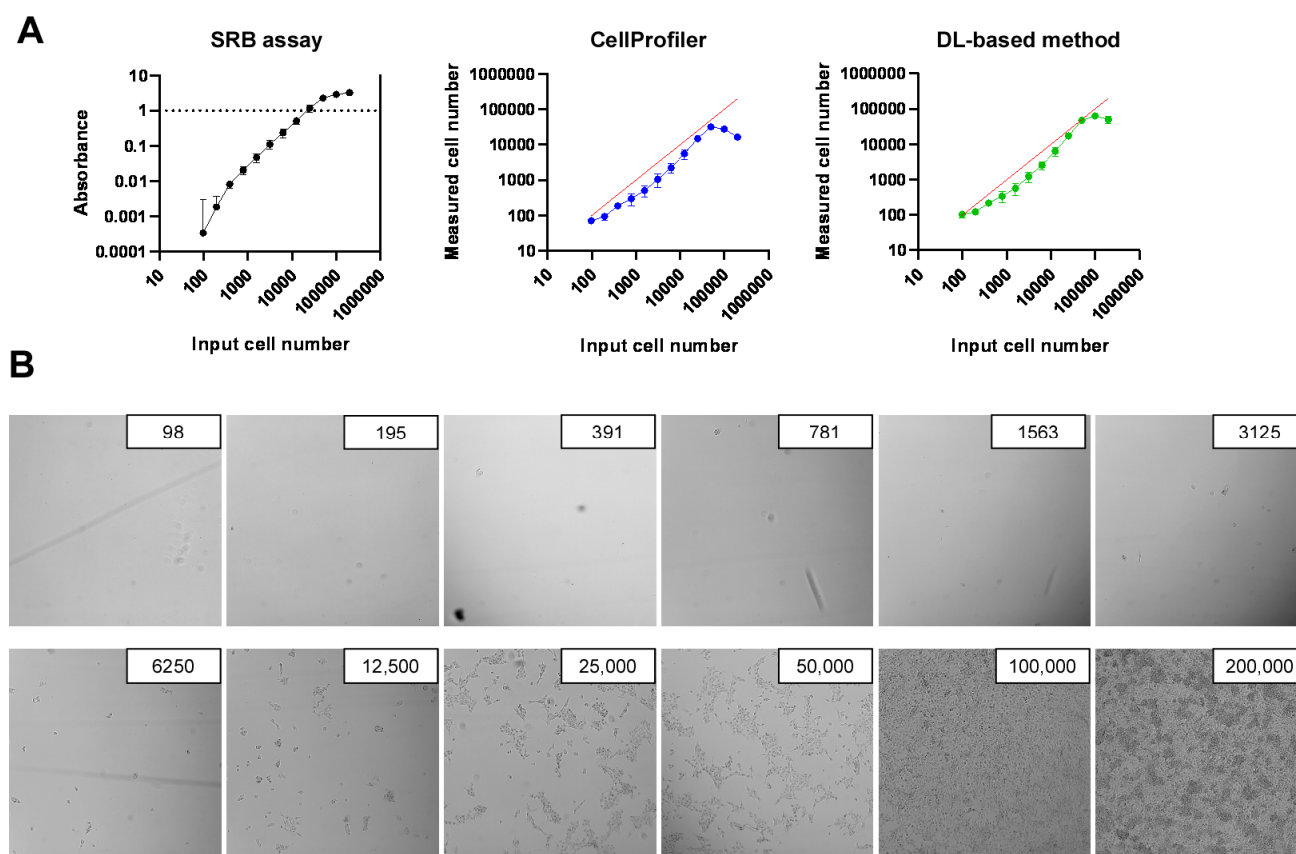


Figure 1. Validation of the methods used to assess cell proliferation. (A) The indicated number of cells were plated in 96-well plates for the SRB assay or PerkinElmer CellCarrier Ultra 96-well plates for the two high-content screening methods. On the following day, either the SRB assay or high-content screening method was conducted. For high-content screening, the nuclei were stained with DAPI, images were segmented using CellProfiler or the deep learning-based method, and nuclei numbers were counted using CellProfiler. The red lines indicate a 45° line, indicating the same number of cells as seeded. (B) Representative phase-contrast images of the wells containing the indicated number of cells. Abbreviations: DL—deep learning.

2.3. Identification of Bacterial Metabolites with Pro and Antiproliferative Properties

The capacity of the bacterial metabolites from the molecule library to modulate the proliferation of 4T1 breast cancer cells was assessed. Cells were treated with five metabolite concentrations spanning the reference concentrations listed in Table 1. Statistical analyses of the dose–response curves were performed independently. We identified seven bioactive metabolites: butyric acid, glycolic acid, D-mannitol, 2,3-butanediol, trans-ferulic acid, 4-hydroxybenzoic acid, vanillic acid, and 3-hydroxyphenylacetic acid (Figure 2). Formic acid displayed antiproliferative properties at the highest concentration; however, the highest concentration of formic acid considerably exceeded the upper end of the reference range (therefore, in Figure 1A, the significance symbol for formic acid is between brackets). However, yric acid, glycolic acid, D-mannitol, 2,3-butanediol, and trans-ferulic acid were antiproliferative at the highest applied concentrations, while 4-hydroxybenzoic acid, vanillic acid, and 3-hydroxyphenylacetic acid supported proliferation at specific concentrations (Figure 2B).

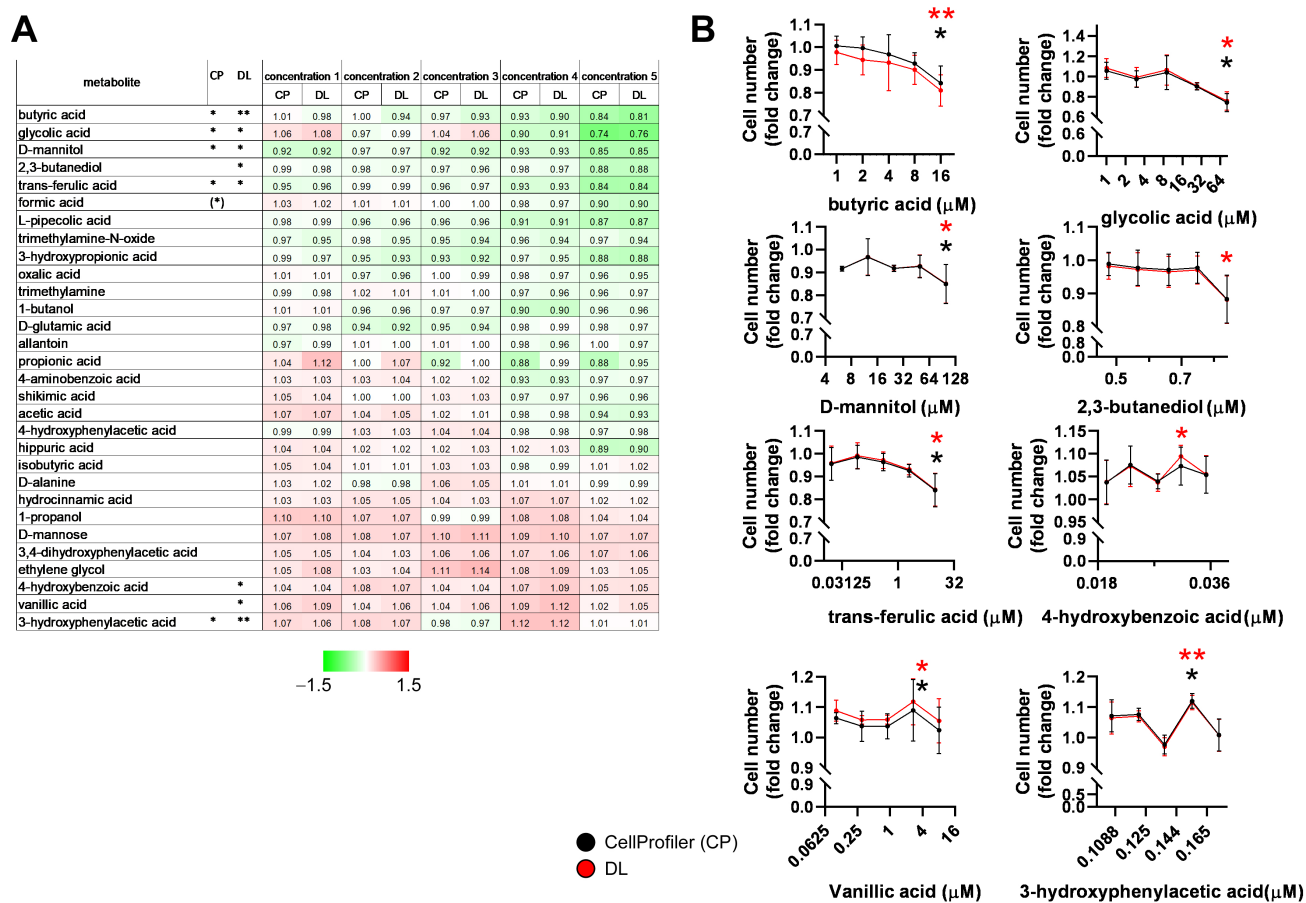


Figure 2. Identification of cytostatic bacterial metabolites in 4T1 breast cancer cells. The cells (800 4T1 cells/well) were plated in PerkinElmer CellCarrier Ultra 96-well plates and treated with the indicated metabolites at the specified concentrations for 48 h. Measurements were repeated at least three times using four technical replicates. Images were acquired and segmented using CellProfiler or the DL algorithm. Nuclei were counted in segmented images using CellProfiler. Data are represented as averages \pm SDs of biological replicates. Values were normalized to vehicle-treated cells and expressed as fold changes. Each metabolite was statistically analyzed separately. (A) A heatmap representation of the effects of the metabolites on 4T1 cell proliferation. (B) The effects of the metabolites on 4T1 cell proliferation. Metabolite concentrations are displayed on the logarithmic axes. * and ** indicate statistically significant differences between vehicle-treated cells (control) and cells treated with the metabolite at $p < 0.05$ and $p < 0.01$, respectively. Abbreviations: DL—deep learning segmentation, CP—CellProfiler’s built-in method segmentation.

2.4. Development of a High-Throughput Method for Assessing Epithelial-to-Mesenchymal Transition

The bacterial metabolites previously identified in breast cancer (lithocholic acid, cadaverine, indole derivatives, and short-chain fatty acids [44]) affected EMT. Therefore, we assessed the effects of members of the metabolite library on EMT. The high-content image analysis methodology was based on the observation that EMT changes cellular morphology in breast cancer [29,84–86]. In parallel, we assessed the protein levels of EMT markers for validation [29,84–86]. As a positive control for the induction of mesenchymal transition, transforming growth factor β (TGF β 10 ng/mL final concentration for 48 h) was applied [87]. As a negative control (inhibition of EMT), we applied SB-431542 (2 μ M final concentration for 48 h), an inhibitor of TGF β superfamily type I activating receptor-like kinases [88]. The protein expression of mesenchymal transition markers (Zinc finger protein SNAI1 (Snail) and vimentin) increased in response to TGF β , while vimentin, but not Snail, decreased in response to SB-431542 treatment in 4T1 cells (Figure 3A). Furthermore, visual

inspection of the cells supported the TGF β -induced mesenchymal and SB-431542-mediated epithelial transition (Figure 3B). In good agreement with these results, TGF β induced increased proportions of mesenchymal cells, while SB-431542 decreased the proportions of mesenchymal cells (Figure 3B), as shown by both high-content screening-based methods. Based on these results, we concluded that the high-content screening-based methods reliably assessed the proportions of epithelial and mesenchymal cells under these conditions.

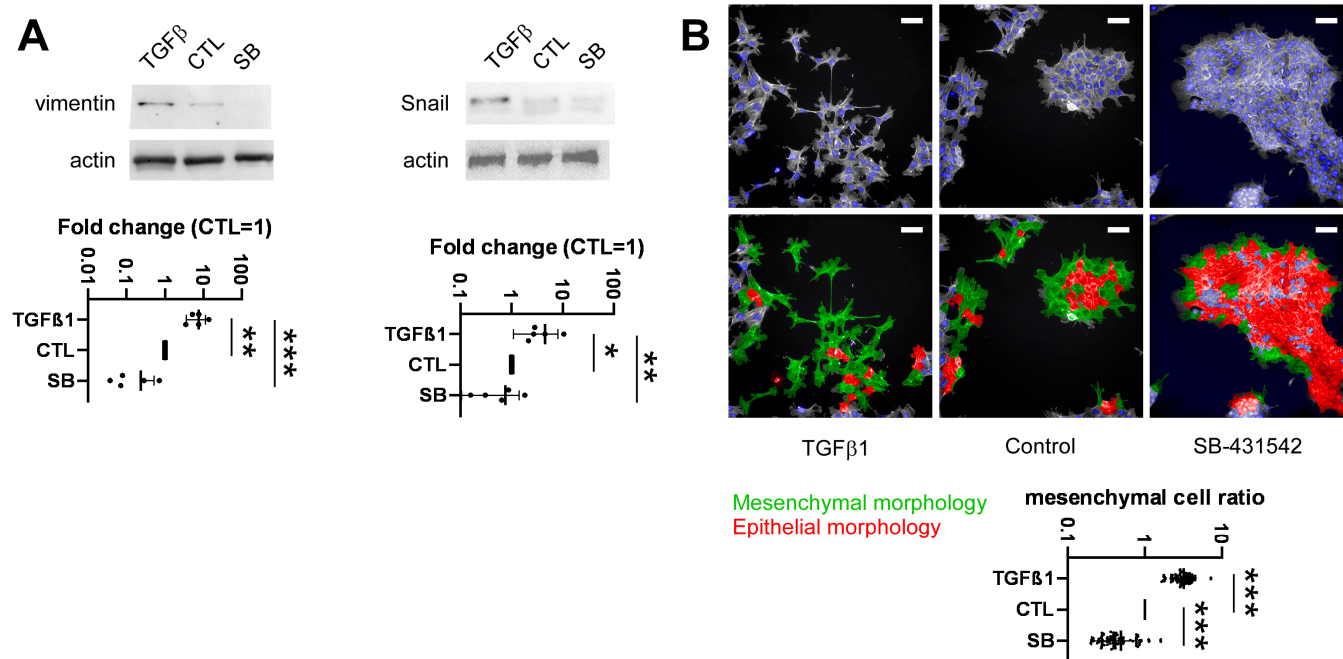


Figure 3. High-content screening-based methods can detect changes in cell morphology and indicate EMT. (A) 1.5×10^6 4T1 cells were plated in Petri dishes and treated with TGF β or SB-431542 for 48 h. Cellular proteins were assessed using Western blotting with the indicated antibodies. Sample blots are shown along with their densitometric evaluation presented as means \pm SD. Values were normalized to vehicle-treated (control) cells. (B) 800 4T1 cells/well were plated in PerkinElmer CellCarrier Ultra 96-well plates and treated with TGF β or SB-431542 for 48 h. Nuclei were stained with DAPI, and cells were visualized using Texas Red-X Phalloidin. The images were segmented using the Harmony software (version 3.1.8) (PerkinElmer, Waltham, MA, USA) to identify cells with epithelial or mesenchymal morphology. Proportions of mesenchymal cells were normalized to total cell number and for inter-sample cell number differences. Normality was tested, and statistical significance was calculated as described in the Methods. Representative fluorescence microscopy images are presented. The scale bar equals 10 μ m. *, **, and *** indicate statistically significant differences between vehicle-treated (control) cells and treated cells at $p < 0.05$, $p < 0.01$, and $p < 0.001$, respectively. Abbreviations: CTL—control, SB—SB-431542, TGF β —transforming growth factor β .

2.5. Identification of Bacterial Metabolites Modulating EMT

Members of the metabolite library were assessed for EMT effects using high-content screening. We identified 3-hydroxyphenylacetic acid, hydrocinnamic acid, 2,3-butanediol, and 4-hydroxybenzoic acid (Figure 4). In all cases, we observed a V-shape curve, where an optimal concentration of the compound significantly reduced the ratio of mesenchymal cells, but lower and higher concentrations were ineffective (Figure 5A). We verified these observations with Western blots. The 4T1 cells were treated with the effective concentration of the metabolites for 48 h, and the protein extracts were probed with anti-Snail and vimentin antibodies. All metabolites, except 2,3-butanediol, reduced the expression of one mesenchymal marker, validating the results of the high-content screening method (Figure 5B). For 2,3-butanediol, we observed a downward trend in the expression of the EMT markers (Figure 5B).

metabolite		CC 1	CC 2	CC 3	CC 4	CC 5
4-hydroxybenzoic acid	**	-0.10	-0.48	-0.25	-0.03	-0.02
2,3-butanediol	**	-0.01	-0.44	0.01	0.04	0.16
hydrocinnamic acid	***	-0.06	-0.38	-0.22	0.01	0.02
3-hydroxyphenylacetic acid	**	-0.15	-0.36	-0.23	-0.10	-0.08
trimethylamine-N-oxide		-0.38	-0.62	-0.43	-0.24	0.17
allantoin		-0.03	-0.36	-0.36	0.02	0.09
1-propanol		-0.11	-0.37	-0.37	0.01	-0.12
D-mannose		-0.27	-0.37	-0.26	-0.05	0.43
isobutyric acid		-0.25	-0.19	-0.32	-0.03	-0.09
D-alanine		0.02	-0.19	-0.28	-0.04	0.01
oxalic acid		0.08	-0.24	-0.11	-0.01	0.14
trimethylamine		0.00	-0.25	-0.26	0.00	-0.13
vanillic acid		0.03	-0.11	-0.24	0.08	0.10
formic acid		-0.04	-0.13	-0.25	0.11	0.07
4-hydroxyphenylacetic acid		-0.01	-0.25	-0.16	0.11	0.04
trans-ferulic acid		0.08	-0.05	-0.12	-0.21	0.25
hippuric acid		0.05	-0.11	-0.17	-0.18	-0.19
3,4-dihydroxyphenylacetic acid		0.03	-0.16	-0.13	-0.05	0.04
D-mannitol		0.02	-0.19	-0.04	-0.05	0.03
L-pipecolic acid		-0.14	-0.14	-0.19	0.08	0.21
D-glutamic acid		-0.04	-0.14	0.03	0.05	0.09
shikimic acid		-0.14	-0.08	-0.02	0.13	0.05
butyric acid		-0.01	-0.06	0.01	0.17	0.14
3-hydroxypropionic acid		-0.10	-0.05	-0.10	-0.07	0.02
1-butanol		-0.12	-0.05	-0.08	0.10	-0.08
propionic acid		0.06	-0.08	0.15	0.19	0.21
4-aminobenzoic acid		-0.07	-0.11	-0.03	0.11	0.05
acetic acid		-0.01	-0.06	0.03	0.13	0.13
ethylene glycol		0.16	-0.05	-0.02	0.38	0.24
glycolic acid		0.02	0.00	-0.08	0.04	0.31



Figure 4. Identification of bioactive bacterial metabolites that suppress EMT. 800 4T1 cells/well were seeded in PerkinElmer CellCarrier Ultra 96-well plates and treated with the indicated metabolites at the concentrations specified in Table 1 for 48 h. The acquired images were segmented using the Harmony software (version 3.1.8) (PerkinElmer) to identify cells with epithelial or mesenchymal morphology. Proportions of the mesenchymal cells were normalized to total cell numbers within a sample and to inter-sample cell number differences. Normality was assessed, and statistical significance was calculated as described in the Methods. Each metabolite was statistically analyzed separately. ** and *** indicate statistically significant differences between vehicle-treated (control) cells and cells treated with a compound at $p < 0.01$ and $p < 0.001$, respectively. Abbreviations: CC 1–5—concentrations indicated in Table 1, the number references increasing doses.

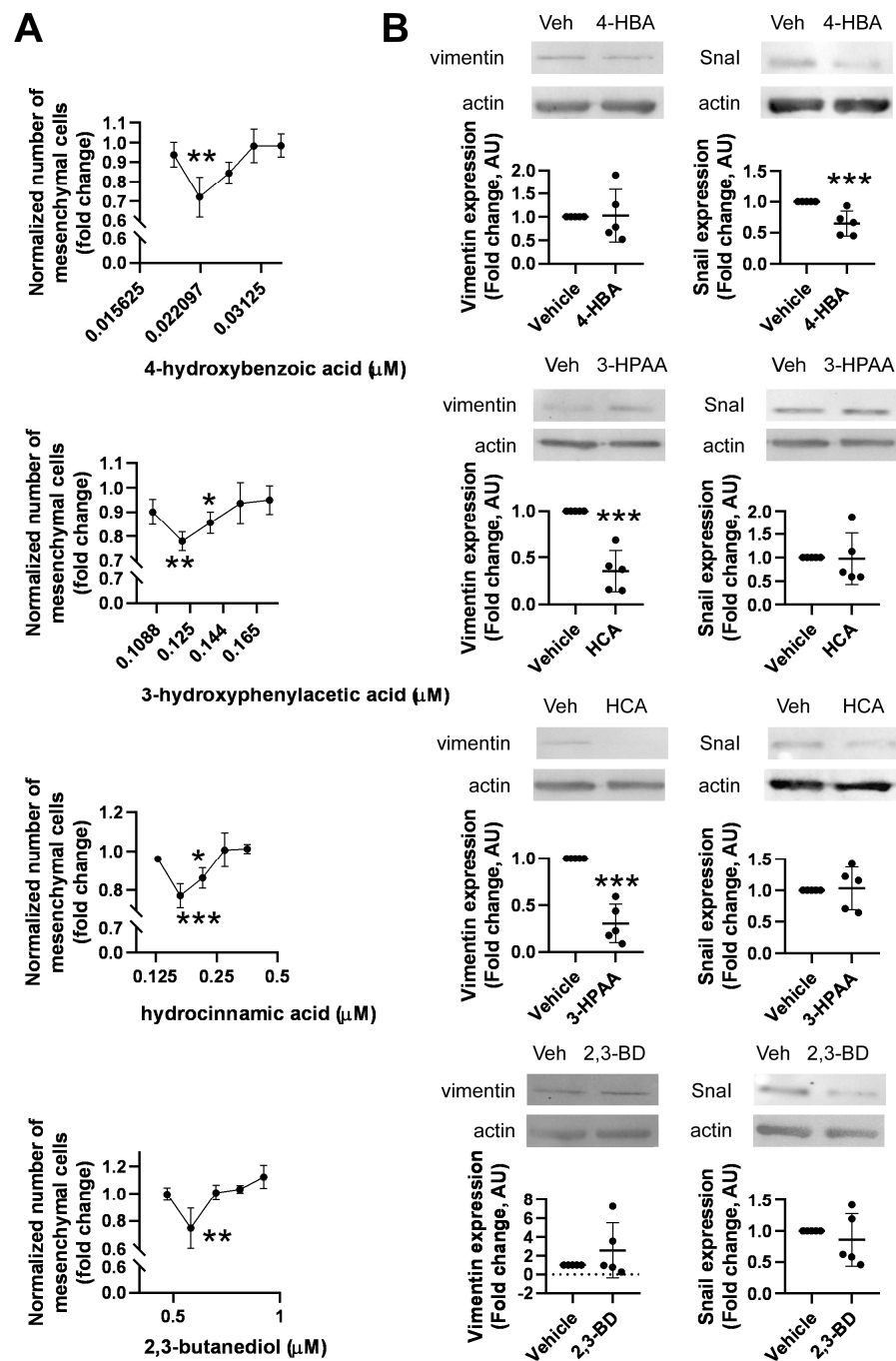


Figure 5. Identification of bioactive bacterial metabolites that suppress EMT. (A) 800 4T1 cells were plated on PerkinElmer CellCarrier Ultra 96-well plates and treated with the indicated metabolites at the concentrations specified in Table 1 for 48 h. The acquired images were segmented using the Harmony software (version 3.1.8) (PerkinElmer) to identify cells with epithelial or mesenchymal morphology. Proportions of the mesenchymal cells were normalized to total cell number within a sample and to inter-sample cell number differences. Normality was assessed, and statistical significance was calculated as described in the Methods. Each metabolite was statistically analyzed separately. (B) 1.5×10^6 4T1 cells were plated in Petri dishes and treated with the indicated metabolites at the concentrations specified in Table 1 for 48 h. Cellular proteins were assessed using Western blotting with the indicated antibodies. Sample blots and densitometry are shown (mean \pm SD). Values were normalized to vehicle-treated (control) cells. *, **, and *** indicate statistically significant differences between vehicle-treated (control) cells and cells treated with a compound at $p < 0.05$, $p < 0.01$, and $p < 0.001$, respectively.

3. Discussion

Bacterial metabolite signaling plays an important role in regulating breast cancer progression [44]. Bioactive bacterial metabolites and toxins elicit multiple effects on breast cancer cells, including DNA instability, changes to cancer cell metabolism, EMT, cell movement, cancer stem cell proportions, cell proliferation, metastasis formation, and modulation of antitumor immune responses (reviewed in [44]). Most bacterial metabolites and toxins are synthesized by the gut microbiome; however, the tumor microbiome may also affect local metabolite and toxin levels (e.g., colibactin [4]). Most bacterial metabolites have antineoplastic features, and enzyme levels responsible for the biosynthesis of these metabolites are lower in breast cancer patients compared to controls (reviewed in [44]).

In this study, we identified nine bioactive metabolites that modulate cell proliferation and inhibit EMT, including butyric acid, vanillic acid, glycolic acid, D-mannitol, trans-ferulic acid, 2,3-butanediol, 4-hydroxybenzoic acid, hydrocinnamic acid, and 3-hydroxyphenylacetic acid (Figure 6A). The chemical nature of the metabolites is diverse, similar to their biochemistry and receptors. Of note, we applied these metabolites in concentrations corresponding to the physiological serum concentrations. The applied concentrations were in the low micromolar or submicromolar range; therefore, it is likely that the data presented here reflect the status of tumors.

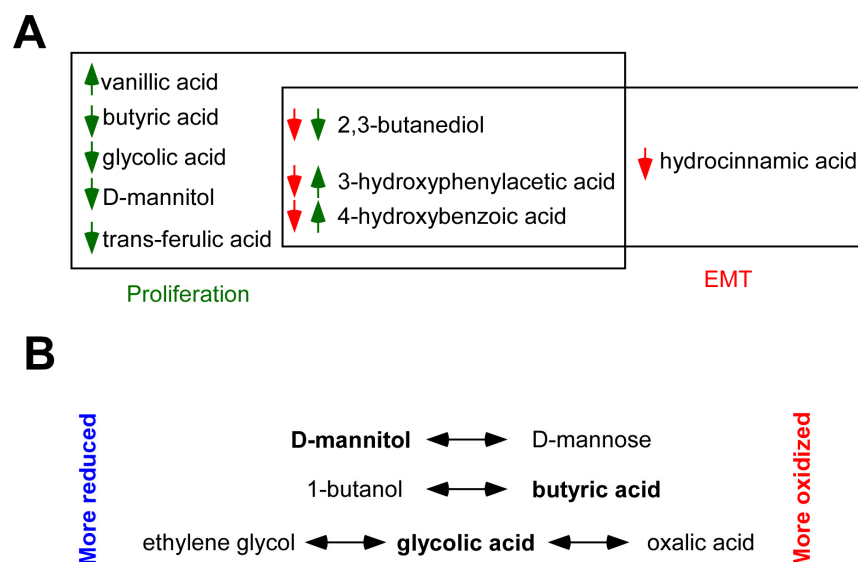


Figure 6. The biological and redox properties of bioactive bacterial metabolites were identified in this study. (A) Venn diagram of the bioactive metabolites highlighting their effects on cell proliferation and EMT. The arrows indicate the direction of changes (up—enhancement, down—inhibition); the green arrows indicate effects on cell proliferation, and the red arrows represent effects on EMT. (B) The schematic representation of the possible effects of the redox potential of the environment on the antiproliferative activity of the metabolites.

Butyric acid and glycolic acid can be classified as short-chain fatty acids. However, yric acid plays multiple roles in breast cancer cells, including inhibitors of histone deacetylases (epigenetic modulators), metabolic substrates, and ligands of free fatty acid receptors (reviewed in [44]). However, yric acid levels decrease in the feces of breast cancer patients [41].

D-mannitol is a polyol, while 2,3-butanediol is a diol. The capacity for 2,3-butanediol synthesis is widespread among bacteria [89,90]. Importantly, 2,3-butanediol suppresses cell proliferation and inhibits EMT. Hence, this compound has the best antineoplastic profile among those assessed in this study.

Interestingly, among short-chain fatty acids and polyols, multiple redox metabolite pairs were identified (D-mannitol—D-mannose, 1-butanol—butyric acid, ethylene glycol—glycolic acid—oxalic acid; the active compounds are in bold); of which only one

partner had cytostatic properties (Figure 6B). These data suggest that the redox environment may influence the bioactivity of the bacterial metabolome/secretome. A recent study showed that in cancers, including breast cancer, ileopathy occurs, leading to slower intestinal passage [82]. Slower passage changes the composition of the microbiome and may also affect the redox balance in the GI tract [83,91].

Amino acid homeostasis is hampered in most breast cancer patients [92,93]. This is reflected by the metabolites identified as bioactive in this study, which are mainly involved in amino acid metabolism. Vanillic acid and trans-ferulic acid are derivatives of L-tyrosine. These metabolites are found in extracts of bacteria or plants tested for anticancer activity. Vanillic acid can act as a pro-oxidant and suppress cell proliferation [94].

Other compounds, such as hydrocinnamic acid, 3-hydroxyphenylacetic acid, and 4-hydroxyphenylacetic acid, contain an aromatic ring and a polar carboxylic acid moiety. Lactic-acid-producing bacteria produce hydrocinnamic acid [95]. The flavonoid compound, 3-hydroxyphenylacetic acid, is generated via the degradation of quercetin derivatives, which are synthesized by *Clostridiales* in the human microbiome [92–99]. The metabolite, 3-hydroxyphenylacetic acid, has cytoprotective features [100] and can bind to the γ -hydroxybutyrate receptor [101,102]. The metabolite, 4-hydroxybenzoic acid, is synthesized from chorismic acid and can bind to the estrogen receptor [103], peroxisome-proliferator-activated receptor (PPAR) γ [104], and G-protein-coupled receptor 40 (GPR40) [104].

Interestingly, multiple metabolites identified in this study, including glycolic acid, hydrocinnamic acid, 2,3-butanediol, 3-hydroxyphenylacetic acid, and 4-hydroxyphenylacetic acid, have antibacterial activity or are involved in quorum sensing [99,103,105–109]. This implies that these metabolites modulate not only the mammary tumor cells but also the microbiome.

Vanillic acid, 4-hydroxybenzoic acid, and 3-hydroxyphenylacetic acid supported proliferation at a specific concentration, i.e., their dose–response curve had an inverted V-shape. This behavior is similar to certain previously identified antineoplastic bacterial metabolites, including indoxyl-sulfate [32] and indol propionic acid [31] (in both cases, V-shape was observed). An inverted V-shape curve indicates the consecutive activation of a receptor-inducing proliferation at low concentrations followed by the activation of another receptor inhibiting proliferation at higher concentrations. Toxicity may also yield similar features at high concentrations; however, the compounds were used in the reference range, making this scenario unlikely.

4. Materials and Methods

4.1. Chemicals

All chemicals were purchased from Sigma (St. Louis, MO, USA) unless stated otherwise. The source of the bacterial metabolites is provided in Table 1. TGF β was from Thermo Scientific (Waltham, MA, USA; Cat. No. #100.21), and SB-431542 was from Sigma (Cat. No. S4317).

4.2. Cell Culture

The 4T1 murine breast cancer cell line was maintained in RPMI-1640 (Sigma) medium, supplemented with 10% fetal bovine serum (FBS), 1% penicillin/streptomycin, 2 mM L-glutamine, and 1% pyruvate at 37 °C with 5% CO₂. A2780 cells were cultured in RPMI 1640 medium supplemented with 10% FBS, 2 mM glutamine, and 1% penicillin-streptomycin. MCF-7 cells were maintained in Minimal Essential Medium (MEM, Sigma), 10% FBS (Sigma), 1% penicillin/streptomycin (Invitrogen, Waltham, MA, USA), and 2 mM L-Glutamine. Capan2 (human pancreatic adenocarcinoma cells) were maintained in MEM (Sigma; cat. no. M8042) containing 10% FBS, 1% penicillin-streptomycin, and 2 mM glutamine at 37 °C with 5% CO₂.

4.3. Cytochemistry and Fluorescent Microscopy

Cells were grown on PerkinElmer CellCarrier Ultra 96-well (Waltham, MA, USA) plates until 70% confluency. Samples were fixed with 4% formaldehyde for 15 min, permeabilized with 1% Triton-X 100, and blocked with 1% BSA/PBS solution. Nuclei were labeled with DAPI (Thermo, Cat. No. R3706) for 5 min. Actin filaments were labeled with Texas Red-X phalloidin (Thermo, T7471) for 1 h. Fluorescent images of the nuclei were acquired at a resolution of 1080×1080 pixels (px) with a $10\times$ objective (N.A. 0.3, $1.196 \mu\text{m}/\text{px}$). DAPI signals (excitation/detection λ : 405/456) were detected in the whole well with 21 fields. Morphology images (i.e., fluorescent detection of phalloidin-stained cells) were acquired at 2160×2160 px image resolution, with a $20\times$ objective (N.A. 0.4, $0.299 \mu\text{m}/\text{px}$). DAPI and Texas Red-X Phalloidin signals (excitation/detection λ : 561/599) were detected in 25 fields from each well. Both image sets were acquired with PerkinElmer Opera Phoenix High Content Screening System (Waltham, MA, USA).

4.4. Cell Morphology Analysis

The acquired images were segmented and analyzed using Harmony 4.8 software (PerkinElmer). The nuclei and the cytoplasm were segmented and textured, and the signal intensity and position of the segmented objects were calculated. Using the calculated morphological properties of TGF β 1-treated, SB-431542-treated, and control cells, an embedded linear regression model was trained to classify the cells into epithelial or mesenchymal morphology groups.

4.5. Training Dataset—DAPI

The training dataset was created from a database of DAPI-stained images from A2780 human ovarian cancer, 4T1 mouse breast cancer, Capan2 human pancreatic cancer, and MCF7 human breast cancer cell lines. Eighty-two images were selected as a training dataset from our image database to provide the highest possible variations in a single image and between images. Images were considered good examples if they had (1) relatively high or low fluorescent signals, (2) contained staining errors or artifacts, or (3) were over-confluent with nuclei of mixed nuclear morphology that covered a part of the well edge. Nuclei were segmented with CellProfiler (Broad Institute, Cambridge, MA, USA) followed by manual correction. The original dataset was augmented using the Albumentations (Python3) library, including 90° rotation, cropping, and brightness changes. The augmentation resulted in 277 pairs of gray-scale images and the corresponding segmented images. The order of the images in the augmented dataset was randomized and split into training, test, and validation sets at a ratio of 80:10:10.

4.6. Training Parameters

Using this dataset, a VGG-UNet segmentation model was trained. The model's architecture was extracted from the Keras-segmentation 0.3.0 library (Python3). The model was trained on a central processing unit for two epochs, eight images per batch through 33 steps. The model used for evaluating the validation dataset had a loss of 0.0512 and an accuracy of 0.9874. The code is shared at the link provided in the "Data Availability" section.

4.7. Nuclei Counting

Nuclei were segmented using Cellprofiler's (<https://cellprofiler.org/>, version 3.1.8) integrated object segmentation method (adaptive Otsu method with three classes—middle class assigned to background). The objects were counted on each image. Parallel to this, the trained semantic segmentation model was applied as a substitute for CellProfiler's segmentation method, followed by object counting with CellProfiler.

4.8. Sulforhodamine B Cell Proliferation Assay

The sulforhodamine B (SRB) assay was used to assess cell proliferation as described in [110,111]. The timing of the proliferation assay was set up as a function of the doubling time of the cell lines.

4.9. Western Blot

Western blotting was performed similar to [112,113]. Briefly, cells and tissues were lysed with RIPA buffer (50 mM Tris, 150 mM NaCl, 0.1% SDS, 1% Nonidet P-40, 1 mM Na₃VO₄, 1 mM NaF, 0.5% sodium deoxycholate, 1 mM phenylmethylsulfonyl fluoride, and protease inhibitor mixture, pH 8.0) and boiled in 50 mM Tris, 2% (*w/v*) SDS, 3.34% (*v/v*) glycerol, and 16.67 mM β-mercaptoethanol. Proteins were separated by 10% SDS-PAGE and transferred onto a nitrocellulose membrane (Bio-Rad Laboratories, Supported, Hercules, CA, USA). Antibodies used in this study were diluted in 5% BSA solution and are shown in Table 2. The secondary antibody was an anti-rabbit IgG HRP-linked antibody (Cell Signaling Technology, Danvers, MA, USA). Labeled proteins were detected using the Chemidoc Touch Imaging System with Supersignal West Pico and Supersignal West Femto ECL Kit (Thermo Fisher Scientific, Waltham, MA, USA). Blots were quantified using densitometry using Image Lab (Bio-Rad) software (version 6.1). All blots are shown in the Supplementary Materials.

Table 2. The antibodies used in the study.

Antibody	Catalog Number	Company	Dilution
Snail	3879S	Cell Signaling Technology	1:1000
Vimentin	5741S		
β-actin	A3854	Sigma	1:20,000

4.10. Statistics

All graphs and statistical analyses were generated using GraphPad Prism v.8.0.1 software. Normality was assessed using the Shapiro–Wilk test. If the dataset was normally distributed or normally distributed after log transformation, one-way ANOVA was applied. If normal distribution was not achieved, the Kruskal–Wallis test was performed. The statistical tests can be accessed in the primary data files. The dose–response curve of the metabolites was subjected to statistical analysis separately for each metabolite. P-values are indicated in the figure captions.

5. Conclusions

In this study, we identified bacterial metabolites that can modulate the behavior of breast cancer cells, similar to hormones. We screened a library of bacterial metabolites and identified nine bioactive metabolites (butyric acid, vanillic acid, glycolic acid, D-mannitol, trans-ferulic acid, 2,3-butanediol, 4-hydroxybenzoic acid, hydrocinnamic acid, and 3-hydroxyphenylacetic acid). The 4T1 murine breast cancer cells were treated with metabolites at concentrations corresponding to the reference serum concentrations of the metabolites. This step is very important to avoid toxicity or off-target effects at supraphysiological concentrations. However, butyric acid, glycolic acid, D-mannitol, 2,3-butanediol, and trans-ferulic acid exerted cytostatic effects, while 3-hydroxyphenylacetic acid, 4-hydroxybenzoic acid, and vanillic acid exerted hyperproliferative effects on 4T1 cells. Furthermore, 3-hydroxyphenylacetic acid, 4-hydroxybenzoic acid, 2,3-butanediol, and hydrocinnamic acid inhibited epithelial-to-mesenchymal transition. We showed that the local redox environment may affect the bioactivity of the metabolites; hence, the local redox potential may affect the bacterial secretome and, consequently, the behavior of breast cancer cells. Out of the nine bioactive metabolites, 2,3-butanediol was the only one with cytostatic and anti-EMT properties. This study suggests that a large portion of the bacterially synthesized metabolites possess bioactivity, and these metabolites can modulate the behavior of cancer cells.

Supplementary Materials: The following supporting information can be downloaded at: <https://www.mdpi.com/article/10.3390/molecules28155898/s1>.

Author Contributions: Conceptualization, G.U., E.M. and P.B.; methodology, A.V., G.U., E.M., P.B., A.S. and E.K.; software, G.U. and P.N.; validation, P.B.; formal analysis, G.U. and E.J.; investigation, G.U., T.K., C.H., S.S. and B.R.; resources, P.B.; data curation, G.U.; writing—original draft preparation, G.U., K.U., P.B. and P.N.; writing—review and editing, G.U., E.M., A.V., P.N. and P.B.; visualization, G.U. and P.B.; supervision, E.M., P.B. and A.S.; project administration, G.U. and P.B.; funding acquisition, P.B. All authors have read and agreed to the published version of the manuscript.

Funding: Our work was supported by grants from NKFIH (K123975, K142141, FK128387), a grant from the Hungarian Academy of Sciences (POST-COVID2021-33), and the Discovery program of the University of Debrecen. Project no. TKP2021-EGA-19 and TKP2021-EGA-20 were implemented with support provided by the National Research, Development, and Innovation Fund of Hungary, financed under the TKP2021-EGA funding scheme. SA and EM were supported by the Bolyai fellowship of the Hungarian Academy of Sciences.

Institutional Review Board Statement: Not applicable.

Informed Consent Statement: Not applicable.

Data Availability Statement: Primary biological data for this manuscript and the code are available at <https://figshare.com/s/8aa8f400a4c73de1d9dd> (DOI: 10.6084/m9.figshare.21394695). Primary images should be solicited from the last author.

Acknowledgments: We are grateful to Kitti Barta and László Finta for the technical assistance.

Conflicts of Interest: Bai is a shareholder and CEO of Holobiont Diagnostics Ltd., which are involved in the development of microbiome-based diagnostic tools. Other authors declare no conflict of interest.

Sample Availability: Not applicable.

References

1. Dafni, U.; Tsourti, Z.; Alatsathianos, I. Breast Cancer Statistics in the European Union: Incidence and Survival across European Countries. *Breast Care* **2019**, *14*, 344–353. [[CrossRef](#)] [[PubMed](#)]
2. Miller, K.D.; Nogueira, L.; Mariotto, A.B.; Rowland, J.H.; Yabroff, K.R.; Alfano, C.M.; Jemal, A.; Kramer, J.L.; Siegel, R.L. Cancer treatment and survivorship statistics, 2019. *CA Cancer J. Clin.* **2019**, *69*, 363–385. [[CrossRef](#)]
3. Thomas, R.M.; Jobin, C. The Microbiome and Cancer: Is the ‘Oncobiome’ Mirage Real? *Trends Cancer* **2015**, *1*, 24–35. [[CrossRef](#)]
4. Urbaniak, C.; Gloor, G.B.; Brackstone, M.; Scott, L.; Tangney, M.; Reid, G. The Microbiota of Breast Tissue and Its Association with Breast Cancer. *Appl. Environ. Microbiol.* **2016**, *82*, 5039–5048. [[CrossRef](#)] [[PubMed](#)]
5. Hieken, T.J.; Chen, J.; Hoskin, T.L.; Walther-Antonio, M.; Johnson, S.; Ramaker, S.; Xiao, J.; Radisky, D.C.; Knutson, K.L.; Kalari, K.R.; et al. The Microbiome of Aseptically Collected Human Breast Tissue in Benign and Malignant Disease. *Sci. Rep.* **2016**, *6*, 30751. [[CrossRef](#)]
6. Chan, A.A.; Bashir, M.; Rivas, M.N.; Duvall, K.; Sieling, P.A.; Pieber, T.R.; Vaishampayan, P.A.; Love, S.M.; Lee, D.J. Characterization of the microbiome of nipple aspirate fluid of breast cancer survivors. *Sci. Rep.* **2016**, *6*, 28061. [[CrossRef](#)] [[PubMed](#)]
7. Meng, S.; Chen, B.; Yang, J.; Wang, J.; Zhu, D.; Meng, Q.; Zhang, L. Study of Microbiomes in Aseptically Collected Samples of Human Breast Tissue Using Needle Biopsy and the Potential Role of in situ Tissue Microbiomes for Promoting Malignancy. *Front. Oncol.* **2018**, *8*, 318. [[CrossRef](#)]
8. Smith, A.; Pierre, J.F.; Makowski, L.; Tolley, E.; Lyn-Cook, B.; Lu, L.; Vidal, G.; Starlard-Davenport, A. Distinct microbial communities that differ by race, stage, or breast-tumor subtype in breast tissues of non-Hispanic Black and non-Hispanic White women. *Sci. Rep.* **2019**, *9*, 11940. [[CrossRef](#)]
9. Tzeng, A.; Sangwan, N.; Jia, M.; Liu, C.-C.; Keslar, K.S.; Downs-Kelly, E.; Fairchild, R.L.; Al-Hilli, Z.; Grobmyer, S.R.; Eng, C. Human breast microbiome correlates with prognostic features and immunological signatures in breast cancer. *Genome Med.* **2021**, *13*, 60. [[CrossRef](#)]
10. Costantini, L.; Magno, S.; Albanese, D.; Donati, C.; Molinari, R.; Filippone, A.; Masetti, R.; Merendino, N. Characterization of human breast tissue microbiota from core needle biopsies through the analysis of multi hypervariable 16S-rRNA gene regions. *Sci. Rep.* **2018**, *8*, 16893. [[CrossRef](#)]
11. Klann, E.; Williamson, J.M.; Tagliamonte, M.S.; Ukhanova, M.; Asirvatham, J.R.; Chim, H.; Yaghjian, L.; Mai, V. Microbiota composition in bilateral healthy breast tissue and breast tumors. *Cancer Causes Control* **2020**, *31*, 1027–1038. [[CrossRef](#)]
12. Thyagarajan, S.; Zhang, Y.; Thapa, S.; Allen, M.S.; Phillips, N.; Chaudhary, P.; Kashyap, M.V.; Vishwanatha, J.K. Comparative analysis of racial differences in breast tumor microbiome. *Sci. Rep.* **2020**, *10*, 14116. [[CrossRef](#)]

13. Wang, H.; Altemus, J.; Niazi, F.; Green, H.; Calhoun, B.C.; Sturgis, C.; Grobmyer, S.R.; Eng, C. Breast tissue, oral and urinary microbiomes in breast cancer. *Oncotarget* **2017**, *8*, 88122–88138. [[CrossRef](#)] [[PubMed](#)]
14. Banerjee, S.; Wei, Z.; Tan, F.; Peck, K.N.; Shih, N.; Feldman, M.; Rebbeck, T.R.; Alwine, J.C.; Robertson, E.S. Distinct microbiological signatures associated with triple negative breast cancer. *Sci. Rep.* **2015**, *5*, 15162. [[CrossRef](#)] [[PubMed](#)]
15. Banerjee, S.; Tian, T.; Wei, Z.; Shih, N.; Feldman, M.D.; Peck, K.N.; DeMichele, A.M.; Alwine, J.C.; Robertson, E.S. Distinct Microbial Signatures Associated With Different Breast Cancer Types. *Front. Microbiol.* **2018**, *9*, 951. [[CrossRef](#)] [[PubMed](#)]
16. Xuan, C.; Shamonki, J.M.; Chung, A.; Dinome, M.L.; Chung, M.; Sieling, P.A.; Lee, D.J. Microbial dysbiosis is associated with human breast cancer. *PLoS ONE* **2014**, *9*, e83744. [[CrossRef](#)] [[PubMed](#)]
17. Nejman, D.; Livyatan, I.; Fuks, G.; Gavert, N.; Zwiang, Y.; Geller, L.T.; Rotter-Maskowitz, A.; Weiser, R.; Mallel, G.; Gigi, E.; et al. The human tumor microbiome is composed of tumor type-specific intracellular bacteria. *Science* **2020**, *368*, 973–980. [[CrossRef](#)] [[PubMed](#)]
18. Thompson, K.J.; Ingle, J.N.; Tang, X.; Chia, N.; Jeraldo, P.R.; Walther-Antonio, M.R.; Kandimalla, K.K.; Johnson, S.; Yao, J.Z.; Harrington, S.C.; et al. A comprehensive analysis of breast cancer microbiota and host gene expression. *PLoS ONE* **2017**, *12*, e0188873. [[CrossRef](#)] [[PubMed](#)]
19. Hogan, G.; Eckenberger, J.; Narayanan, N.; Walker, S.P.; Claesson, M.J.; Corrigan, M.; O’Hanlon, D.; Tangney, M. Biopsy bacterial signature can predict patient tissue malignancy. *Sci. Rep.* **2021**, *11*, 18535. [[CrossRef](#)]
20. Banerjee, S.; Wei, Z.; Tian, T.; Bose, D.; Shih, N.N.C.; Feldman, M.D.; Khoury, T.; De Michele, A.; Robertson, E.S. Prognostic correlations with the microbiome of breast cancer subtypes. *Cell Death Dis.* **2021**, *12*, 831. [[CrossRef](#)]
21. Giallourou, N.; Urbaniak, C.; Puebla-Barragan, S.; Vorkas, P.A.; Swann, J.R.; Reid, G. Characterizing the breast cancer lipidome and its interaction with the tissue microbiota. *Commun. Biol.* **2021**, *4*, 1229. [[CrossRef](#)] [[PubMed](#)]
22. Goedert, J.J.; Jones, G.; Hua, X.; Xu, X.; Yu, G.; Flores, R.; Falk, R.T.; Gail, M.H.; Shi, J.; Ravel, J.; et al. Investigation of the association between the fecal microbiota and breast cancer in postmenopausal women: A population-based case-control pilot study. *J. Natl. Cancer Inst.* **2015**, *107*, djv147. [[CrossRef](#)] [[PubMed](#)]
23. Byrd, D.A.; Vogtmann, E.; Wu, Z.; Han, Y.; Wan, Y.; Clegg-Lampsey, J.-N.; Yarney, J.; Wiafe-Addai, B.; Wiafe, S.; Awuah, B.; et al. Associations of fecal microbial profiles with breast cancer and non-malignant breast disease in the Ghana Breast Health Study. *Int. J. Cancer* **2021**, *148*, 2712–2723. [[CrossRef](#)] [[PubMed](#)]
24. Zhu, J.; Liao, M.; Yao, Z.; Liang, W.; Li, Q.; Liu, J.; Yang, H.; Ji, Y.; Wei, W.; Tan, A.; et al. Breast cancer in postmenopausal women is associated with an altered gut metagenome. *Microbiome* **2018**, *6*, 136. [[CrossRef](#)]
25. Howe, C.; Kim, S.J.; Mitchell, J.; Im, E.; Kim, Y.S.; Kim, Y.S.; Rhee, S.H. Differential expression of tumor-associated genes and altered gut microbiome with decreased *Akkermansia muciniphila* confer a tumor-preventive microenvironment in intestinal epithelial Pten-deficient mice. *Biochim. Biophys. Acta-Mol. Basis Dis.* **2018**, *1864*, 3746–3758. [[CrossRef](#)]
26. Fruge, A.D.; Van der Pol, W.; Rogers, L.Q.; Morrow, C.D.; Tsuruta, Y.; Demark-Wahnefried, W. Fecal *Akkermansia muciniphila* Is Associated with Body Composition and Microbiota Diversity in Overweight and Obese Women with Breast Cancer Participating in a Presurgical Weight Loss Trial. *J. Acad. Nutr. Diet.* **2018**, *9*, 164. [[CrossRef](#)]
27. Wu, A.H.; Tseng, C.; Vigen, C.; Yu, Y.; Cozen, W.; Garcia, A.A.; Spicer, D. Gut microbiome associations with breast cancer risk factors and tumor characteristics: A pilot study. *Breast Cancer Res. Treat.* **2020**, *182*, 451–463. [[CrossRef](#)]
28. Luu, T.H.; Michel, C.; Bard, J.M.; Dravet, F.; Nazih, H.; Bobin-Dubigeon, C. Intestinal Proportion of *Blautia* sp. is Associated with Clinical Stage and Histoprognostic Grade in Patients with Early-Stage Breast Cancer. *Nutr. Cancer* **2017**, *69*, 267–275. [[CrossRef](#)]
29. Miko, E.; Vida, A.; Kovacs, T.; Ujlaki, G.; Trencsenyi, G.; Marton, J.; Sari, Z.; Kovacs, P.; Boratkó, A.; Hujber, Z.; et al. Lithocholic acid, a bacterial metabolite reduces breast cancer cell proliferation and aggressiveness. *Biochim. Biophys. Acta-Bioenerg.* **2018**, *1859*, 958–974. [[CrossRef](#)]
30. Kovács, T.; Mikó, E.; Vida, A.; Sebő, É.; Toth, J.; Csonka, T.; Boratkó, A.; Ujlaki, G.; Lente, G.; Kovács, P.; et al. Cadaverine, a metabolite of the microbiome, reduces breast cancer aggressiveness through trace amino acid receptors. *Sci. Rep.* **2019**, *9*, 1300. [[CrossRef](#)]
31. Sári, Z.; Mikó, E.; Kovács, T.; Jankó, L.; Csonka, T.; Sebő, E.; Toth, J.; Tóth, D.; Árkosy, P.; Boratkó, A.; et al. Indolepropionic acid, a metabolite of the microbiome, has cytostatic properties in breast cancer by activating AHR and PXR receptors and inducing oxidative stress. *Cancers* **2020**, *12*, 2411. [[CrossRef](#)]
32. Sári, Z.; Mikó, E.; Kovács, T.; Boratkó, A.; Ujlaki, G.; Jankó, L.; Kiss, B.; Uray, K.; Bai, P. Indoxylsulfate, a Metabolite of the Microbiome, Has Cytostatic Effects in Breast Cancer via Activation of AHR and PXR Receptors and Induction of Oxidative Stress. *Cancers* **2020**, *12*, 2915. [[CrossRef](#)] [[PubMed](#)]
33. Sári, Z.; Kovács, T.; Csonka, T.; Török, M.; Sebő, É.; Toth, J.; Tóth, D.; Mikó, E.; Kiss, B.; Szeőcs, D.; et al. Fecal expression of *E. coli* lysine decarboxylase (LdcC) is downregulated in E-cadherin negative lobular breast carcinoma. *Physiol. Int.* **2020**, *107*, 349–358. [[CrossRef](#)]
34. Murray, W.R.; Blackwood, A.; Calman, K.C.; MacKay, C. Faecal bile acids and clostridia in patients with breast cancer. *Br. J. Cancer* **1980**, *42*, 856–860. [[CrossRef](#)]
35. Goedert, J.J.; Hua, X.; Bielecka, A.; Okayasu, I.; Milne, G.L.; Jones, G.S.; Fujiwara, M.; Sinha, R.; Wan, Y.; Xu, X.; et al. Postmenopausal breast cancer and oestrogen associations with the IgA-coated and IgA-noncoated faecal microbiota. *Br. J. Cancer* **2018**, *23*, 435. [[CrossRef](#)]

36. Bobin-Dubigeon, C.; Luu, H.T.; Leuillet, S.; Lavergne, S.N.; Carton, T.; Le Vacon, F.; Michel, C.; Nazih, H.; Bard, J.M. Faecal Microbiota Composition Varies between Patients with Breast Cancer and Healthy Women: A Comparative Case-Control Study. *Nutrients* **2021**, *13*, 2705. [CrossRef]
37. Horigome, A.; Okubo, R.; Hamazaki, K.; Kinoshita, T.; Katsumata, N.; Uezono, Y.; Xiao, J.Z.; Matsuoka, Y.J. Association between blood omega-3 polyunsaturated fatty acids and the gut microbiota among breast cancer survivors. *Benef. Microbes* **2019**, *10*, 751–758. [CrossRef]
38. Terrisse, S.; Derosa, L.; Iebba, V.; Ghiringhelli, F.; Vaz-Luis, I.; Kroemer, G.; Fidelle, M.; Christodoulidis, S.; Segata, N.; Thomas, A.M.; et al. Intestinal microbiota influences clinical outcome and side effects of early breast cancer treatment. *Cell Death Differ.* **2021**, *28*, 2778–2796. [CrossRef]
39. Hou, M.F.; Ou-Yang, F.; Li, C.L.; Chen, F.M.; Chuang, C.H.; Kan, J.Y.; Wu, C.C.; Shih, S.L.; Shiao, J.P.; Kao, L.C.; et al. Comprehensive profiles and diagnostic value of menopausal-specific gut microbiota in premenopausal breast cancer. *Exp. Mol. Med.* **2021**, *53*, 1636–1646. [CrossRef] [PubMed]
40. Wu, A.H.; Vigen, C.; Tseng, C.; Garcia, A.A.; Spicer, D. Effect of chemotherapy and weight change on the gut microbiome of breast cancer patients during the first year of treatment. *Res. Sq.* **2022**, *14*, 433–451. Available online: <https://www.researchsquare.com/article/rs-970564/v970561> (accessed on 30 June 2023). [CrossRef] [PubMed]
41. Zhu, Q.; Zai, H.; Zhang, K.; Zhang, X.; Luo, N.; Li, X.; Hu, Y.; Wu, Y. L-norvaline affects the proliferation of breast cancer cells based on the microbiome and metabolome analysis. *J. Appl. Microbiol.* **2022**, *133*, 1014–1026. [CrossRef]
42. He, C.; Liu, Y.; Ye, S.; Yin, S.; Gu, J. Changes of intestinal microflora of breast cancer in premenopausal women. *Eur. J. Clin. Microbiol. Infect. Dis.* **2021**, *40*, 503–513. [CrossRef] [PubMed]
43. An, J.; Kim, J.B.; Yang, E.Y.; Kim, H.O.; Lee, W.-H.; Yang, J.; Kwon, H.; Paik, N.S.; Lim, W.; Kim, Y.-K.; et al. Bacterial extracellular vesicles affect endocrine therapy in MCF7 cells. *Medicine* **2021**, *100*, e25835. [CrossRef] [PubMed]
44. Kovács, T.; Mikó, E.; Ujlaki, G.; Yousef, H.; Csontos, V.; Uray, K.; Bai, P. The involvement of oncobiosis and bacterial metabolite signaling in metastasis formation in breast cancer. *Cancer Metastasis Rev.* **2021**, *40*, 1223–1249. [CrossRef]
45. Wilmanski, T.; Rappaport, N.; Earls, J.C.; Magis, A.T.; Manor, O.; Lovejoy, J.; Omenn, G.S.; Hood, L.; Gibbons, S.M.; Price, N.D. Blood metabolome predicts gut microbiome alpha-diversity in humans. *Nat. Biotechnol.* **2019**, *37*, 1217–1228. [CrossRef]
46. Miko, E.; Kovacs, T.; Sebo, E.; Toth, J.; Csonka, T.; Ujlaki, G.; Sipos, A.; Szabo, J.; Mehes, G.; Bai, P. Microbiome-Microbial Metabolome-Cancer Cell Interactions in Breast Cancer-Familiar, but Unexplored. *Cells* **2019**, *8*, E293. [CrossRef] [PubMed]
47. Kumari, S.; Malla, R.R. Recent advances in metabolomics of triple negative breast cancer. *Breast J.* **2020**, *26*, 498–501. [CrossRef]
48. Hill, M.J.; Goddard, P.; Williams, R.E. Gut bacteria and aetiology of cancer of the breast. *Lancet* **1971**, *2*, 472–473. [CrossRef]
49. Kovács, P.; Csonka, T.; Kovács, T.; Sári, Z.; Ujlaki, G.; Sipos, A.; Karányi, Z.; Szeőcs, D.; Hegedűs, C.; Uray, K.; et al. Lithocholic acid, a metabolite of the microbiome, increases oxidative stress in breast cancer. *Cancers* **2019**, *11*, 1255. [CrossRef]
50. Yonezawa, T.; Kobayashi, Y.; Obara, Y. Short-chain fatty acids induce acute phosphorylation of the p38 mitogen-activated protein kinase/heat shock protein 27 pathway via GPR43 in the MCF-7 human breast cancer cell line. *Cell. Signal.* **2007**, *19*, 185–193. [CrossRef]
51. Thirunavukkarasan, M.; Wang, C.; Rao, A.; Hind, T.; Teo, Y.R.; Siddiquee, A.A.; Goghari, M.A.I.; Kumar, A.P.; Herr, D.R. Short-chain fatty acid receptors inhibit invasive phenotypes in breast cancer cells. *PLoS ONE* **2017**, *12*, e0186334. [CrossRef]
52. Liebich, H.M.; Buelow, H.J.; Kallmayer, R. Quantification of endogenous aliphatic alcohols in serum and urine. *J. Chromatogr.* **1982**, *239*, 343–349. [CrossRef] [PubMed]
53. Montgomery, J.A.; Jetté, M.; Brunengraber, H. Assay of physiological levels of 2,3-butanediol diastereomers in blood and urine by gas chromatography-mass spectrometry. *Anal. Biochem.* **1990**, *185*, 71–76. [CrossRef] [PubMed]
54. Feliciano, R.P.; Istas, G.; Heiss, C.; Rodriguez-Mateos, A. Plasma and Urinary Phenolic Profiles after Acute and Repetitive Intake of Wild Blueberry. *Molecules* **2016**, *21*, 1120. [CrossRef] [PubMed]
55. Izzo, J.L., Jr.; Greulich, D. Radioenzymatic assay for plasma dihydroxyphenylglycol (DHPG), dihydroxymandelic acid (DOMA) and dihydroxyphenylacetic acid (DOPAC). *Life Sci.* **1983**, *33*, 483–488. [CrossRef]
56. Novarino, G.; El-Fishawy, P.; Kayserili, H.; Meguid, N.A.; Scott, E.M.; Schroth, J.; Silhavy, J.L.; Kara, M.; Khalil, R.O.; Ben-Omran, T.; et al. Mutations in BCKD-kinase lead to a potentially treatable form of autism with epilepsy. *Science* **2012**, *338*, 394–397. [CrossRef]
57. Lianidou, E.S.; Ioannou, P.C. Simple spectrofluorometric determination of p-aminobenzoic and p-aminosalicylic acids in biological fluids by use of terbium-sensitized luminescence. *Clin. Chem.* **1996**, *42*, 1659–1665. [CrossRef]
58. Richards, R.H.; Dowling, J.A.; Vreman, H.J.; Feldman, C.; Weiner, M.W. Acetate levels in human plasma. *Proc. Clin. Dial. Transpl. Forum* **1976**, *6*, 73–79.
59. Jakobsdottir, G.; Bjerregaard, J.H.; Skovbjerg, H.; Nyman, M. Fasting serum concentration of short-chain fatty acids in subjects with microscopic colitis and celiac disease: No difference compared with controls, but between genders. *Scand. J. Gastroenterol.* **2013**, *48*, 696–701. [CrossRef]
60. Koh, A.; De Vadder, F.; Kovatcheva-Datchary, P.; Backhed, F. From Dietary Fiber to Host Physiology: Short-Chain Fatty Acids as Key Bacterial Metabolites. *Cell* **2016**, *165*, 1332–1345. [CrossRef]
61. Shafaei, A.; Vamathevan, V.; Pandohee, J.; Lawler, N.G.; Broadhurst, D.; Boyce, M.C. Sensitive and quantitative determination of short-chain fatty acids in human serum using liquid chromatography mass spectrometry. *Anal. Bioanal. Chem.* **2021**, *413*, 6333–6342. [CrossRef] [PubMed]

62. Kand'ár, R.; Záková, P. Allantoin as a marker of oxidative stress in human erythrocytes. *Clin. Chem. Lab. Med.* **2008**, *46*, 1270–1274. [[CrossRef](#)]
63. Pavitt, D.V.; de Fonseca, S.; Al-Khalaf, N.; Cam, J.M.; Reaveley, D.A. Assay of serum allantoin in humans by gas chromatography-mass spectrometry. *Clin. Chim. Acta Int. J. Clin. Chem.* **2002**, *318*, 63–70. [[CrossRef](#)] [[PubMed](#)]
64. Gruber, J.; Tang, S.Y.; Jenner, A.M.; Mudway, I.; Blomberg, A.; Behndig, A.; Kasiman, K.; Lee, C.Y.; Seet, R.C.; Zhang, W.; et al. Allantoin in human plasma, serum, and nasal-lining fluids as a biomarker of oxidative stress: Avoiding artifacts and establishing real in vivo concentrations. *Antioxid. Redox Signal.* **2009**, *11*, 1767–1776. [[CrossRef](#)] [[PubMed](#)]
65. Lin, C.-H.; Yang, H.-T.; Chiu, C.-C.; Lane, H.-Y. Blood levels of D-amino acid oxidase vs. D-amino acids in reflecting cognitive aging. *Sci. Rep.* **2017**, *7*, 14849. [[CrossRef](#)]
66. Pitkänen, E.; Pitkänen, O.; Uotila, L. Enzymatic determination of unbound D-mannose in serum. *Eur. J. Clin. Chem. Clin. Biochem. J. Forum Eur. Clin. Chem. Soc.* **1997**, *35*, 761–766. [[CrossRef](#)]
67. Campi, B.; Codini, S.; Bisoli, N.; Baldi, S.; Zucchi, R.; Ferrannini, E.; Saba, A. Quantification of d-mannose in plasma: Development and validation of a reliable and accurate HPLC-MS-MS method. *Clin. Chim. Acta* **2019**, *493*, 31–35. [[CrossRef](#)]
68. Taguchi, T.; Miwa, I.; Mizutani, T.; Nakajima, H.; Fukumura, Y.; Kobayashi, I.; Yabuuchi, M.; Miwa, I. Determination of d-Mannose in Plasma by HPLC. *Clin. Chem.* **2003**, *49*, 181–183. [[CrossRef](#)]
69. Baumann, K.; Angerer, J. Occupational chronic exposure to organic solvents. VI. Formic acid concentration in blood and urine as an indicator of methanol exposure. *Int. Arch. Occup. Environ. Health* **1979**, *42*, 241–249. [[CrossRef](#)]
70. Marangella, M.; Petrarulo, M.; Bianco, O.; Vitale, C.; Finocchiaro, P.; Linari, F. Glycolate determination detects type I primary hyperoxaluria in dialysis patients. *Kidney Int.* **1991**, *39*, 149–154. [[CrossRef](#)]
71. Nowak, P.J.; Wilk, R.; Prymont-Przyminska, A.; Zwolinska, A.; Sarniak, A.; Wlodarczyk, A.; de Graft-Johnson, J.; Mamelka, B.; Zasowska-Nowak, A.; Bartnicki, P.; et al. Hemodialysis Decreases the Concentration of Accumulated Plant Phenols in the Plasma of Patients on Maintenance Dialysis: Influence of Residual Renal Function. *Ther. Apher. Dial.* **2017**, *21*, 572–585. [[CrossRef](#)] [[PubMed](#)]
72. Afessa, B.; Mullon, J.; Badley, A.; Gajic, O. The impact of protocolized sepsis order set on the process of care in patients with severe sepsis/septic shock. *Crit. Care* **2007**, *11*, P6. [[CrossRef](#)]
73. Baas, J.C.; van de Laar, R.; Dorland, L.; Duran, M.; Berger, R.; Poll-The, B.T.; de Koning, T.J. Plasma pipercolic acid is frequently elevated in non-peroxisomal disease. *J. Inher. Metab. Dis.* **2002**, *25*, 699–701. [[CrossRef](#)] [[PubMed](#)]
74. Psychogios, N.; Hau, D.D.; Peng, J.; Guo, A.C.; Mandal, R.; Bouatra, S.; Sinelnikov, I.; Krishnamurthy, R.; Eisner, R.; Gautam, B.; et al. The human serum metabolome. *PLoS ONE* **2011**, *6*, e16957. [[CrossRef](#)] [[PubMed](#)]
75. Zaremski, P.M.; Hodgkinson, A. The fluorimetric determination of oxalic acid in blood and other biological materials. *Biochem. J.* **1965**, *96*, 717–721. [[CrossRef](#)] [[PubMed](#)]
76. Sreekumar, A.; Poisson, L.M.; Rajendiran, T.M.; Khan, A.P.; Cao, Q.; Yu, J.; Laxman, B.; Mehra, R.; Lonigro, R.J.; Li, Y.; et al. Metabolomic profiles delineate potential role for sarcosine in prostate cancer progression. *Nature* **2009**, *457*, 910–914. [[CrossRef](#)] [[PubMed](#)]
77. Bain, M.A.; Faull, R.; Fornasini, G.; Milne, R.W.; Evans, A.M. Accumulation of trimethylamine and trimethylamine-N-oxide in end-stage renal disease patients undergoing haemodialysis. *Nephrol. Dial. Transplant.* **2006**, *21*, 1300–1304. [[CrossRef](#)]
78. Bahado-Singh, R.O.; Akolekar, R.; Mandal, R.; Dong, E.; Xia, J.; Kruger, M.; Wishart, D.S.; Nicolaidis, K. Metabolomics and first-trimester prediction of early-onset preeclampsia. *J. Matern. Fetal Neonatal Med.* **2012**, *25*, 1840–1847. [[CrossRef](#)]
79. Garcia, E.; Wolak-Dinsmore, J.; Wang, Z.; Li, X.S.; Bennett, D.W.; Connelly, M.A.; Otvos, J.D.; Hazen, S.L.; Jeyarajah, E.J. NMR quantification of trimethylamine-N-oxide in human serum and plasma in the clinical laboratory setting. *Clin. Biochem.* **2017**, *50*, 947–955. [[CrossRef](#)]
80. Nie, J.; Xie, L.; Zhao, B.X.; Li, Y.; Qiu, B.; Zhu, F.; Li, G.F.; He, M.; Wang, Y.; Wang, B.; et al. Serum Trimethylamine N-Oxide Concentration Is Positively Associated With First Stroke in Hypertensive Patients. *Stroke* **2018**, *49*, 2021–2028. [[CrossRef](#)]
81. Randrianarisoa, E.; Lehn-Stefan, A.; Wang, X.; Hoene, M.; Peter, A.; Heinzmann, S.S.; Zhao, X.; Königsrainer, I.; Königsrainer, A.; Balletshofer, B.; et al. Relationship of Serum Trimethylamine N-Oxide (TMAO) Levels with early Atherosclerosis in Humans. *Sci. Rep.* **2016**, *6*, 26745. [[CrossRef](#)] [[PubMed](#)]
82. Yonekura, S.; Terrisse, S.; Alves Costa Silva, C.; Lafarge, A.; Iebba, V.; Ferrere, G.; Goubet, A.G.; Fahrner, J.E.; Lahmar, I.; Ueda, K.; et al. Cancer induces a stress ileopathy depending on B-adrenergic receptors and promoting dysbiosis that contribute to carcinogenesis. *Cancer Discov.* **2021**, *12*, 1128–1151. [[CrossRef](#)]
83. Malik, A.; Morya, R.K.; Bhadada, S.K.; Rana, S. Type 1 diabetes mellitus: Complex interplay of oxidative stress, cytokines, gastrointestinal motility and small intestinal bacterial overgrowth. *Eur. J. Clin. Investig.* **2018**, *48*, e13021. [[CrossRef](#)]
84. Kalluri, R.; Weinberg, R.A. The basics of epithelial-mesenchymal transition. *J. Clin. Investig.* **2009**, *119*, 1420–1428. [[CrossRef](#)] [[PubMed](#)]
85. Lamouille, S.; Xu, J.; Derynck, R. Molecular mechanisms of epithelial-mesenchymal transition. *Nat. Rev. Mol. Cell Biol.* **2014**, *15*, 178–196. [[CrossRef](#)] [[PubMed](#)]
86. González-Martínez, S.; Pérez-Mies, B.; Pizarro, D.; Caniego-Casas, T.; Cortés, J.; Palacios, J. Epithelial Mesenchymal Transition and Immune Response in Metaplastic Breast Carcinoma. *Int. J. Mol. Sci.* **2021**, *22*, 7398. [[CrossRef](#)]
87. Trelford, C.B.; Dagnino, L.; Di Guglielmo, G.M. Transforming growth factor- β in tumour development. *Front. Mol. Biosci.* **2022**, *9*, 991612. [[CrossRef](#)]

88. Inman, G.J.; Nicolás, F.J.; Callahan, J.F.; Harling, J.D.; Gaster, L.M.; Reith, A.D.; Laping, N.J.; Hill, C.S. SB-431542 is a potent and specific inhibitor of transforming growth factor-beta superfamily type I activin receptor-like kinase (ALK) receptors ALK4, ALK5, and ALK7. *Mol. Pharmacol.* **2002**, *62*, 65–74. [[CrossRef](#)]
89. Ng, C.; Jung, M.-y.; Lee, J.; Oh, M.-K. Production of 2,3-butanediol in *Saccharomyces cerevisiae* by in silico aided metabolic engineering. *Microb. Cell Factories* **2012**, *11*, 68. [[CrossRef](#)]
90. Garg, S.K.; Jain, A. Fermentative production of 2,3-butanediol: A review. *Bioresour. Technol.* **1995**, *51*, 103–109. [[CrossRef](#)]
91. Million, M.; Tidjani Alou, M.; Khelaifia, S.; Bachar, D.; Lagier, J.C.; Dione, N.; Brah, S.; Hugon, P.; Lombard, V.; Armougom, F.; et al. Increased Gut Redox and Depletion of Anaerobic and Methanogenic Prokaryotes in Severe Acute Malnutrition. *Sci. Rep.* **2016**, *6*, 26051. [[CrossRef](#)]
92. Cha, Y.J.; Kim, E.S.; Koo, J.S. Amino Acid Transporters and Glutamine Metabolism in Breast Cancer. *Int. J. Mol. Sci.* **2018**, *19*, 907. [[CrossRef](#)] [[PubMed](#)]
93. Geck, R.C.; Toker, A. Nonessential amino acid metabolism in breast cancer. *Adv. Biol. Regul.* **2016**, *62*, 11–17. [[CrossRef](#)] [[PubMed](#)]
94. Pessoa, A.S.; Tokuhara, C.K.; Fakhoury, V.S.; Pagnan, A.L.; Oliveira, G.S.N.; Sanches, M.L.R.; Inacio, K.K.; Costa, B.C.; Ximenes, V.F.; Oliveira, R.C. The dimerization of methyl vanillate improves its effect against breast cancer cells via pro-oxidant effect. *Chem. Biol. Interact.* **2022**, *361*, 109962. [[CrossRef](#)]
95. Rouxel, M.; Barthe, M.; Marchand, P.; Juin, C.; Mondamert, L.; Berges, T.; Blanc, P.; Verdon, J.; Berjeaud, J.M.; Aucher, W. Characterization of antifungal compounds produced by lactobacilli in cheese-mimicking matrix: Comparison between active and inactive strains. *Int. J. Food Microbiol.* **2020**, *333*, 108798. [[CrossRef](#)] [[PubMed](#)]
96. Aura, A.M.; O’Leary, K.A.; Williamson, G.; Ojala, M.; Bailey, M.; Puupponen-Pimiä, R.; Nuutila, A.M.; Oksman-Caldentey, K.M.; Poutanen, K. Quercetin Derivatives Are Deconjugated and Converted to Hydroxyphenylacetic Acids but Not Methylated by Human Fecal Flora in Vitro. *J. Agric. Food Chem.* **2002**, *50*, 1725–1730. [[CrossRef](#)]
97. Rechner, A.R.; Smith, M.A.; Kuhnle, G.; Gibson, G.R.; Debnam, E.S.; Srai, S.K.S.; Moore, K.P.; Rice-Evans, C.A. Colonic metabolism of dietary polyphenols: Influence of structure on microbial fermentation products. *Free Radic. Biol. Med.* **2004**, *36*, 212–225. [[CrossRef](#)]
98. Williamson, G.; Clifford, M.N. Role of the small intestine, colon and microbiota in determining the metabolic fate of polyphenols. *Biochem. Pharmacol.* **2017**, *139*, 24–39. [[CrossRef](#)]
99. Ozdemir, O.O.; Soyer, F. *Pseudomonas aeruginosa* Presents Multiple Vital Changes in Its Proteome in the Presence of 3-Hydroxyphenylacetic Acid, a Promising Antimicrobial Agent. *ACS Omega* **2020**, *5*, 19938–19951. [[CrossRef](#)]
100. Liu, Y.; Myojin, T.; Li, K.; Kurita, A.; Seto, M.; Motoyama, A.; Liu, X.; Satoh, A.; Munemasa, S.; Murata, Y.; et al. A Major Intestinal Catabolite of Quercetin Glycosides, 3-Hydroxyphenylacetic Acid, Protects the Hepatocytes from the Acetaldehyde-Induced Cytotoxicity through the Enhancement of the Total Aldehyde Dehydrogenase Activity. *Int. J. Mol. Sci.* **2022**, *23*, 1762. [[CrossRef](#)]
101. Chen, W.; Wu, H.; Hernandez, R.J.; Mehta, A.K.; Ticku, M.K.; France, C.P.; Coop, A. Ethers of 3-hydroxyphenylacetic acid as selective gamma-hydroxybutyric acid receptor ligands. *Bioorganic Med. Chem. Lett.* **2005**, *15*, 3201–3202. [[CrossRef](#)] [[PubMed](#)]
102. Ticku, M.K.; Mehta, A.K. Characterization and Pharmacology of the GHB Receptor. *Ann. N. Y. Acad. Sci.* **2008**, *1139*, 374–385. [[CrossRef](#)] [[PubMed](#)]
103. Pugazhendhi, D.; Pope, G.S.; Darbre, P.D. Oestrogenic activity of p-hydroxybenzoic acid (common metabolite of paraben esters) and methylparaben in human breast cancer cell lines. *J. Appl. Toxicol.* **2005**, *25*, 301–309. [[CrossRef](#)] [[PubMed](#)]
104. Rosiles-Alanis, W.; Zamilpa, A.; García-Macedo, R.; Zavala-Sánchez, M.A.; Hidalgo-Figueroa, S.; Mora-Ramiro, B.; Román-Ramos, R.; Estrada-Soto, S.E.; Almanza-Perez, J.C. 4-Hydroxybenzoic Acid and β -Sitosterol from Cucurbita ficifolia Act as Insulin Secretagogues, Peroxisome Proliferator-Activated Receptor-Gamma Agonists, and Liver Glycogen Storage Promoters: In Vivo, In Vitro, and In Silico Studies. *J. Med. Food* **2022**, *25*, 588–596. [[CrossRef](#)] [[PubMed](#)]
105. Valle-González, E.R.; Jackman, J.A.; Yoon, B.K.; Mokrzecka, N.; Cho, N.J. pH-Dependent Antibacterial Activity of Glycolic Acid: Implications for Anti-Acne Formulations. *Sci. Rep.* **2020**, *10*, 7491. [[CrossRef](#)]
106. Sousa, M.; Afonso, A.C.; Teixeira, L.S.; Borges, A.; Saavedra, M.J.; Simões, L.C.; Simões, M. Hydrocinnamic Acid and Perillyl Alcohol Potentiate the Action of Antibiotics against *Escherichia coli*. *Antibiotics* **2023**, *12*, 360. [[CrossRef](#)]
107. Sharma, S.; Gopu, V.; Sivasankar, C.; Shetty, P.H. Hydrocinnamic acid produced by *Enterobacter xiangfangensis* impairs AHL-based quorum sensing and biofilm formation in *Pseudomonas aeruginosa*. *RSC Adv.* **2019**, *9*, 28678–28687. [[CrossRef](#)]
108. Chen, Y.; Chen, Y.; Liu, L.; Zhang, Y.; Yuan, J. Microbial synthesis of 4-hydroxybenzoic acid from renewable feedstocks. *Food Chem. Mol. Sci.* **2021**, *3*, 100059. [[CrossRef](#)]
109. Dillon, V.M. Natural Anti-Microbial Systems | Preservative Effects During Storage. In *Encyclopedia of Food Microbiology*, 2nd ed.; Batt, C.A., Tortorello, M.L., Eds.; Academic Press: Oxford, UK, 2014; pp. 941–947.
110. Kacsir, I.; Sipos, A.; Bényei, A.; Janka, E.; Buglyó, P.; Somsak, L.; Bai, P.; Bokor, É. Reactive oxygen species production is responsible for antineoplastic activity of osmium, ruthenium, iridium and rhodium half-sandwich type complexes with bidentate glycosyl hetero-cyclic ligands in various cancer cell models. *Int. J. Mol. Sci.* **2022**, *23*, 813. [[CrossRef](#)]
111. Skehan, P.; Storeng, R.; Scudiero, D.; Monks, A.; McMahon, J.; Vistica, D.; Warren, J.T.; Bokesch, H.; Kenney, S.; Boyd, M.R. New colorimetric cytotoxicity assay for anticancer-drug screening. *J. Natl. Cancer Inst.* **1990**, *82*, 1107–1112. [[CrossRef](#)]

112. Marton, J.; Fodor, T.; Nagy, L.; Vida, A.; Kis, G.; Brunyanszki, A.; Antal, M.; Luscher, B.; Bai, P. PARP10 (ARTD10) modulates mitochondrial function. *PLoS ONE* **2018**, *13*, e0187789. [[CrossRef](#)] [[PubMed](#)]
113. Marton, J.; Peter, M.; Balogh, G.; Bodi, B.; Vida, A.; Szanto, M.; Bojcsuk, D.; Janko, L.; Bhattoa, H.P.; Gombos, I.; et al. Poly(ADP-ribose) polymerase-2 is a lipid-modulated modulator of muscular lipid homeostasis. *Biochim. Biophys. Acta-Mol. Cell Biol. Lipids* **2018**, *1863*, 1399–1412. [[CrossRef](#)] [[PubMed](#)]

Disclaimer/Publisher’s Note: The statements, opinions and data contained in all publications are solely those of the individual author(s) and contributor(s) and not of MDPI and/or the editor(s). MDPI and/or the editor(s) disclaim responsibility for any injury to people or property resulting from any ideas, methods, instructions or products referred to in the content.